Structural effects of Sr substitution in $La_{2-x}Sr_xNiO_{4+\delta}$

P. J. Heaney*
Princeton Materials Institute and Department of Geosciences, Princeton University, Princeton, New Jersey 08544

A. Mehta
Stanford Synchrotron Radiation Laboratory, Stanford Linear Accelerator Center, Stanford, California 94309

G. Sarosi, V. E. Lamberti, and A. Navrotsky
Princeton Materials Institute and Department of Geosciences, Princeton University, Princeton, New Jersey 08544
(Received 13 June 1997)

Structures within the $La_{2-x}Sr_xNiO_{4+\delta}$ system ($0<x\leq 1$) were refined by Rietveld analysis of powder x-ray-diffraction data. Our results reveal three distinct regimes that parallel energetic transformations within the series. For $0\leq x<0.2$, enthalpies of oxidation are strongly exothermic and the compounds are monophasic and orthorhombic. Hole saturation occurs for $0.2<x<0.6$, and the symmetry decreases from orthorhombic to monoclinic. For $0.6<x<1.0$, diffraction patterns suggest phase immiscibility between a Sr-poor, hole-saturated compound and a Sr-rich phase for which oxidation is strongly favored. Fourier synthesis maps for all compositions revealed evidence for microtwinning and positional disorder among apical oxygen atoms. [S0163-1829(98)06118-9]

I. INTRODUCTION

Pure La_2CuO_4 and La_2NiO_4 are antiferromagnetic insulators with K_2NiF_4-type structures. Acceptor doping, via either substitution of Sr^{2+} for La^{3+} or insertion of interstitial oxygen, transforms both phases to a metallic state. The insulator-to-metal transition occurs for a much higher formal valence of nickel than for copper, but the most striking difference in the electronic behavior of the two Sr-doped series is that the metallic state of $(La,Sr)_2CuO_4$ exhibits unambiguous superconductivity with increasing Sr concentration (up to a maximum T_c of 35 K for $x=0.15$), whereas evidence for superconductivity within the metallic state of $(La,Sr)_2NiO_{4+\delta}$ is tenuous.[1–3] This disparity is somewhat surprising for isostructural compounds based on adjacent transition metal elements.

Scientists have closely examined the effects of acceptor doping in the nickelate series in the hope that an understanding of the apparent absence of superconductivity may explain its occurrence among the cuprates. Calorimetric investigations by DiCarlo *et al.*[4] have revealed two major discontinuities in the partial molar enthalpies of oxidation for the Ba- and Sr-substituted lanthanum nickelates (Fig. 1). They find that for $0\leq x<0.2$, the enthalpies of oxidation are exothermic and approximately -215 ± 50 kJ/mol of O_2. For $0.2<x<0.6$, the enthalpies are nearly 0, with an estimated maximum error of ± 100 kJ/mol of O_2. Finally, for $0.6<x\leq 1.0$, the enthalpies of oxidation again are exothermic and around -280 ± 50 kJ/mol of O_2.

DiCarlo *et al.* measured the enthalpy of oxidation associated with an increase in excess oxygen (δ) by ~ 0.04. Thus their calorimetric measurements reflect the energetic cost of incorporating small amounts of additional oxygen within the structure or, equivalently, the ease with which additional holes are created. The thermochemical results obtained by these authors are not consistent with a simple model of oxidation energetics. The incorporation of oxygen into a structure generally requires energy when oxygen enters the structure as an interstitial (i.e., when $\delta>0$), whereas energy is liberated when oxygen atoms fill vacancies (i.e., when $\delta<0$). Excess oxygen content in $La_{2-x}Sr_xNiO_{4+\delta}$ decreases with increasing Sr substitution,[4–6] and thus the enthalpy of oxidation is expected to decrease (i.e., become more exothermic) with increasing x, perhaps discontinuously when $\delta=0$ and the oxidation mechanism changes.

In the study of DiCarlo *et al.*, $La_{2-x}Sr_xNiO_{4+\delta}$ transforms from having an excess to a deficiency of oxygen near $x=0.2$, and these authors do observe a discontinuity in the enthalpy of oxidation at this point. However, the nature of the discontinuity runs counter to expectations in that the enthalpy becomes dramatically *less* exothermic with higher Sr

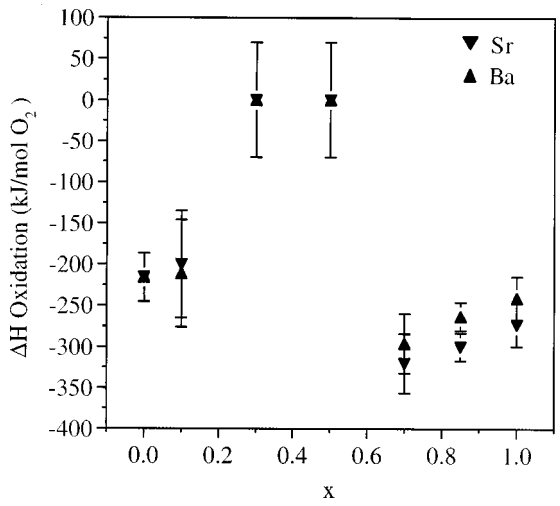

FIG. 1. Dependence of the enthalpy of oxidation on x in $La_{2-x}A_xNiO_{4+\delta}$ with $A=$ Sr and Ba, based on data presented in DiCarlo *et al.* (Ref. 4).

content. Their results suggest that the incorporation of oxygen (and of holes) is energetically much less favorable in the regime for which $0.2<x<0.6$ than for $0<x<0.2$. By contrast, a second discontinuity at $x=0.6$ suggests that oxidation again is a strongly exothermic process for large Sr contents, so that the incorporation of excess holes in $La_{2-x}Sr_xNiO_{4+\delta}$ for $0.6<x<1.0$ is energetically favored.

These thermochemical anomalies are accompanied by discontinuities in a number of physical properties as a function of increasing Sr concentration. For example, the variations of the unit cell parameters a and c reverse sign at $x=0.5$.[2,5,7] The dependence of resistivity on Sr content exhibits an abrupt shift in slope at either $x=0.2$ (Ref. 6) or at $x=0.5$ (Ref. 2) or at both $x=0.25$ and $x=0.5$ (Ref. 5) at room temperature. The dependence of the Seebeck coefficient on x changes sign at $x=0.5$ at room temperature.[5,6] Last, the excess oxygen concentration (δ) not only reverses sign, but changes slope at $x=0.2$.[4–6]

The discontinuities in thermochemical and electromagnetic properties along the $La_2NiO_{4+\delta}$-$LaSrNiO_{4+\delta}$ join suggest that this series comprises several electronically distinct regimes. For the present investigation, we attempted to determine whether the physical discontinuities separating these regimes are correlated with structural transformations within the nickelate system. If so, then the different electronic regimes may represent thermodynamically distinct phases. Although the general structural behavior of this series has been known for decades,[2,5,7] these compounds have been modeled after the idealized K_2NiF_4 isotype, and efforts to unravel the defect chemistry of this series have focused on the first thermochemical regime for which $0<x<0.2$.[1,3,8–10]

In our study, structures of five compositions within the $La_{2-x}Sr_xNiO_{4+\delta}$ system ($0<x<1$) were refined by Rietveld analysis of powder x-ray-diffraction data. Because the structure of $La_2NiO_{4+\delta}$ is known to exhibit an extreme sensitivity to slight variations in dopant and oxygen concentrations,[11] the samples used in the present study derived from the same material used in the thermochemical experiments of DiCarlo *et al.*[4] This practice ensures a measure of confidence in the direct comparison of our structural results with the thermochemical data of DiCarlo *et al.*

II. EXPERIMENTAL METHODS

A. Synthesis

The synthesis of the $La_{2-x}Sr_xNiO_{4+\delta}$ compounds as performed by DiCarlo *et al.*[4] is described as follows: Stoichiometric amounts of La_2O_3 (Aesar 99.99%, dried at 700 °C prior to use), $SrCO_3$ (Aesar 99.99%, dried at 130 °C prior to use), and NiO (Aesar 99.999%) were ground in an agate mortar and heated in a platinum crucible at 1100 °C for 12 h. After heating, the samples were ground again and heated at 1250 °C for 24 h, then annealed at 704 °C in air for 24 h, and quenched to room temperature.

B. Electron probe microanalysis

Powdered samples were impregnated in epoxy and examined with a Cameca SX-50 microprobe. The microprobe was operated with an accelerating voltage of 15 kV and a regulated current of 20 nA. Calibration standards included LaB_6 for La, $SrTiO_3$ for Sr, NiO for Ni, and Al_2O_3 as the standard for O. Composition and oxygen stoichiometry measurements were performed using energy dispersive spectrometry (EDS) with a Li-drifted Si solid-state x-ray detector. Counting times for the EDS spectra were 20 s for peak positions and 10 s for background.

C. Iodometric titration

The oxygen contents ($4+\delta$) of the final products were determined through iodometric titration against KIO_3-standardized $Na_2S_2O_3$. At least three titrations were performed for each composition; the errors are taken at the 95% confidence level. It should be emphasized that the errors reflect only the propagated statistical uncertainties of the titrations and exclude systematic errors arising from, for example, uncertainties in the assumed cation stoichiometry or the concentration of titrant.

D. X-ray-powder-diffraction data collection

Diffraction patterns were collected from samples with the following Sr contents: $x=0.1$, 0.3, 0.5, 0.7, 0.85, and 1.0. All of the samples were ground under acetone with an agate mortar and pestle and then smeared on to zero-background quartz plates. Diffraction experiments were conducted with a Scintag PAD V automated powder diffractometer using Cu $K\alpha$ x rays and an intrinsic Ge solid-state detector. Step scans of spun samples ranged from 15 to 120° 2θ with step sizes of 0.03° 2θ and count times of 10 s per step. Phase purity was confirmed in all samples but $x=0.85$. Extra diffraction peaks produced by this sample could be assigned to unreacted NiO and $SrCO_3$; EDS analysis also detected high levels of these impurities, and this composition was omitted from the study.

E. Structure refinements

After data collection, Rietveld refinement was performed with the general structure analysis system (GSAS) of Larson and von Dreele.[12] Starting parameters for all compositions were taken from the synchrotron x-ray-diffraction study of $La_2NiO_{4.18}$ of Mehta and Heaney,[13] and all refinements followed the same sequence. The first stages of analysis included background (up to 12 refinable coefficients in a cosine Fourier series), scale factor, sample shift, and lattice parameters. Once these parameters had converged, the peak profiles were fitted to symmetric pseudo-Voigt functions with a peak asymmetry correction. A previous refinement of a LaB_6 standard (NIST SRM 660) provided starting values for Gaussian and Lorentzian coefficients, and only the Lorentzian components and a Gaussian particle size coefficient were varied.

Upon convergence of the above parameters, atom positions, isotropic temperature factors, and site occupancies for La, Sr, Ni, and apical O were refined. Site fractions for La and Sr were constrained to sum to unity. Refinement of basal oxygen atoms yielded divergent results, presumably due to positional disorder over two general positions. Observed Fourier synthesis maps revealed site splitting within the (001) plane with no evidence for displacement from this plane. When basal oxygen atoms were located with half-occupancy on the split sites indicated by the observed Fou-

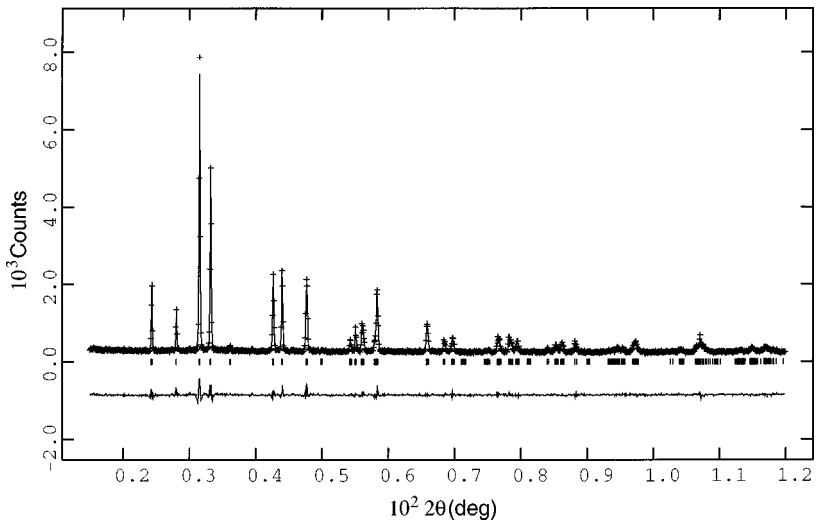

FIG. 2. Observed (crosses) and calculated (line) diffraction pattern with difference curve (bottom) based on Rietveld analysis of powder x-ray-diffraction data for Sr(0.5).

rier synthesis maps, the oxygen atoms refined towards the special positions and the refinements ultimately diverged, even with heavy positional damping. Consequently, basal oxygen atoms were located on special positions without refinement for all compositions. Likewise, excess oxygen positions were noted on observed Fourier maps, but their positional parameters did not refine stably due to their small occupancies. A comparison of observed and calculated diffraction patterns is presented in Fig. 2.

III. RESULTS AND DISCUSSION

A. Compositional analysis

Microprobe analyses confirmed that the La-Sr ratios of the synthetic powders fell within $\sim 5\%$ of the nominal values, with the exception of Sr(0.85), which was not included in this study. Iodometric titration confirmed a steady decrease in oxygen content with increased Sr substitution (Fig. 3). The oxygen stoichiometries obtained in this study are in excellent agreement with the values reported by Granados *et al.*[6] However, as noted by these and other authors,[14–16] iodometric titration does not always provide an accurate measure of the oxygen content due to end-point detection problems and uncertainties in anion valency. Therefore, values determined by DiCarlo *et al.*[4] for these samples using H_2 reduction are presented in Fig. 3. Although the absolute oxygen contents measured by the two techniques are slightly different, the trends are the same. In particular, a break in slope at $x=0.2$ is clearly evident in the titration data, in agreement with previous studies.[5,6]

In Fig. 3, we also include the formal Ni valence ($=2+x+2\delta$) as a function of Sr content, assuming that the valence of La$=+3$, Sr$=+2$, and O$=-2$. To the extent that the discontinuities observed along the $La_2NiO_{4+\delta}$-$LaSrNiO_{4+\delta}$ join are electronically driven, the total hole content within these compounds may be more significant than solely the degree of Sr substitution. Indeed, samples having the same Sr contents often have slightly different hole concentrations due to variations in final oxygenation treatments during sample preparation. These disparities in the total hole concentration may account for the small shifts in the values of x that demarcate the ''electronic boundaries'' reported by different investigators.

B. Symmetry breaking with increasing Sr content

The K_2NiO_4 isotype belongs to space group $I4/mmm$, and many structural studies have assumed tetragonal symmetry for various members of the (La,Sr)-nickelate series,[1,6,8,17] including one Rietveld analysis of $La_{2-x}Sr_xNiO_{4.00}$ for $0 \leqslant x \leqslant 1.6$.[7] On the other hand, Jorgensen *et al.*[18] have argued that $La_2NiO_{4.18}$ possesses orthorhombic symmetry at 295 K on the basis of systematic peak broadening in powder neutron-diffraction data. By analogy with $La_2CuO_{4+\delta}$, they assumed that the real symmetry of $La_2NiO_{4.18}$ must be $Bmab$, which

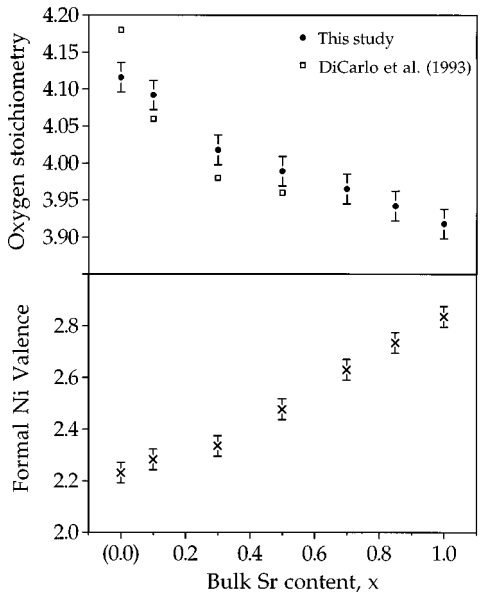

FIG. 3. Variation of oxygen content with Sr substitution (top) and formal Ni valence (bottom) as determined by iodometric titration (dark circles). Squares represent oxygen contents determined using H_2 reduction by DiCarlo *et al.* (Ref. 4).

TABLE I. Hamilton R_{wp} analysis for $La_{2-x}Sr_xNiO_{4+\delta}$.

Sr(x)		$F4/mmm$	$Fmmm$	$F112/m$
	χ^2	1.642	1.630	1.630
0.1	R_{wp}	6.90	6.87	6.87
	R_{wp} ratio	1.004	1.000	
	$R_{1,3480,0.005}$	1.001	1.001	
	χ^2	1.484	1.430	1.422
0.3	R_{wp}	6.54	6.41	6.39
	R_{wp} ratio	1.020	1.003	
	$R_{1,3480,0.005}$	1.001	1.001	
	χ^2	1.820	1.621	1.453
0.5	R_{wp}	7.25	6.84	6.47
	R_{wp} ratio	1.060	1.056	
	$R_{1,3480,0.005}$	1.001	1.001	

departs from the tetragonal isotype through the displacement of basal oxygen atoms from the 001 plane parallel to c.

More recently, Mehta and Heaney[13] observed orthorhombic peak splitting in a powder synchrotron x-ray-diffraction study of $La_2NiO_{4.18}$. Fourier synthesis maps based on Rietveld analysis of the data revealed in-plane separation of the basal oxygen positions, but no displacement of the basal oxygen atoms from the 001 planes. Based on these Fourier syntheses, we suggested that $Fmmm$ describes the average symmetry for $La_2NiO_{4.18}$, but on a local scale the symmetry corresponds to space group $Bbcm$ and not $Bmab$.

In the present study of Sr-doped nickelates, all compositions refined stably with tetragonal symmetry. However, we observed that the quality of the refinement decreased with increasing x, and the peak profiles systematically broadened with increasing x. Although our conventional sealed-tube x-ray configuration did not reveal distinct peak splitting, it seemed likely that our refinement results reflected a decrease in symmetry with increased Sr concentration. In order to test this interpretation, we refined the structures for the entire composition range in three different space group symmetries: $F4/mmm$, $Fmmm$, and $F112/m$. The unconventional settings were used to facilitate comparisons with the $Fmmm$ setting as employed by previous authors.[18]

We then compared the goodnesses of fit for the different symmetries using Hamilton's significance test[19] based on the weighted profile residuals R_{wp}, as is appropriate for powder diffraction data (see Prince[20]). Lowering the symmetry from $F4/mmm$ to $Fmmm$ requires the addition of only one variable (the lattice parameter b). Further reduction in symmetry to $F112/m$ was performed with only one additional parameter, the monoclinic angle γ. Although the $F112/m$ structure contains two crystallographically distinct basal oxygen atoms, these atoms occupy special sites with no refinable positional parameters. For our refinements, we constrained these basal oxygen atoms to have the same isotropic temperature factors.

The results of this analysis are presented in Table I, and they reveal a change in structural symmetry at $x \sim 0.2$. For $La_{1.9}Sr_{0.1}NiO_{4+\delta}$, refinement in an orthorhombic space group yielded a better fit than did a tetragonal space group at a 99.5% confidence level, but lowering the symmetry to the monoclinic space group did not meaningfully improve the fit. On the other hand, for $x > 0.2$, refinement in $F112/m$ did lower the goodness of fit significantly at the 99.5% confidence level, and the degree of improvement increased with increasing x. However, refinements of data for $x > 0.2$ in the triclinic space group $F\ 1$ were unstable and did not improve the fit. Although we attempted to match the improvement obtained by decreasing symmetry through modifications of the tetragonal refinement (such as by incorporation of strain effects), no tetragonal models yielded comparable fits with as few additional parameters.

We conclude that the proper symmetry for $La_{2-x}Sr_xNiO_{4+\delta}$ is monoclinic for $x > 0.2$, and our final refined lattice parameters, atom positions, and bond distances are presented in Tables II, III, and IV, respectively. The results reveal that the discontinuities associated with enthalpy of oxidation, excess oxygen incorporation, and resistivity appear to coincide with a change in symmetry from orthorhombic to monoclinic. Because the thermochemical measurements of DiCarlo *et al.*[4] exhibit an abrupt increase in the enthalpy of oxidation (and a corresponding decrease in hole stability) with increasing Sr content at $x = 0.2$, it seems likely that the monoclinic distortion of $La_{2-x}Sr_xNiO_{4+\delta}$ is electronically driven.

C. Positional disorder among the basal oxygen atoms

For all compositions in the $La_{2-x}Sr_xNiO_{4+\delta}$ system refined in this study, observed Fourier (F_{obs}) synthesis maps parallel to (001) revealed positional disorder among both the basal oxygen and the apical oxygen atoms of the NiO_6 octahedra (Figs. 4 and 5), as was also described in Mehta and Heaney[13] for end member $La_2NiO_{4.18}$. In this earlier study, we interpreted the O_{basal} splitting as evidence for microtwinned domains, denoted as *d* and *l* twins, which result from clockwise and counterclockwise rotation of the NiO_6 octahedra about the c axis.

The behavior of the basal oxygen atoms in the present analysis was nearly identical to that observed in $La_2NiO_{4.18}$. Attempts to refine basal oxygen atoms in the sites indicated by the electron density distributions led to divergent results, as occurred previously with the synchrotron data. Nevertheless, the calculated Ni-O_{basal} bond lengths based on the centroids of the split electron densities at (0.25, 0.25, 0) and

TABLE II. Unit cell and refinement data for $La_{2-x}Sr_xNiO_{4+\delta}$.

	Sr(0)[a]	Sr(0.1)	Sr(0.3)	Sr(0.5)	Sr(0.7) Phase 1 49 wt. %	Sr(0.7) Phase 2 51 wt. %	Sr(1.0) Phase 1 12 wt. %	Sr(1.0) Phase 2 88 wt. %
Space group	*Fmmm*	*Fmmm*	*F*112/*m*	*F*112/*m*	*F*112/*m*	*F*112/*m*	*F*112/*m*	*F*112/*m*
a (Å)	5.46520(7)	5.4454(1)	5.4145(1)	5.3893(2)	5.3921(2)	5.4054(2)	5.3901(6)	5.4108(2)
b (Å)	5.46869(7)	5.4484(1)	5.4185(1)	5.3995(2)	5.3931(2)	5.4044(2)	5.3911(6)	5.4118(2)
c (Å)	12.6780(2)	12.6949(2)	12.7150(2)	12.7317(3)	12.6958(8)	12.5878(8)	12.680(2)	12.3786(7)
γ (deg)	90	90	90.029(3)	90.100(3)	90.093(9)	90.196(7)	90.06(3)	90.03(1)
Volume (Å^3)	378.92(1)	376.64(1)	373.04(1)	370.49(1)	369.19(1)	367.72(1)	368.44(2)	362.46(2)
ρ (g/cm^3)	6.940	6.898	6.773	6.533	6.402	6.369	6.288	6.212
No. obs.		3499	3499	3499	3665		3449	
R_{wp}		0.0687	0.0639	0.0647	0.0800		0.0739	
χ^2	1.987	1.630	1.422	1.453	2.416		2.583	

[a]From Mehta and Heaney (Ref. 13).

TABLE III. Atom positions for $La_{2-x}Sr_xNiO_{4+\delta}$.

Sr(x)		La	Sr	Ni	O_{apical}	$O_{basal}(1)$	$O_{basal}(2)$
	x	0	0	0	0	0.25	
	y	0	0	0	0	0.25	
0.1	z	0.3614(1)	0.3614(1)	0	0.1745(10)	0.0	
	Frac	0.88(2)	0.12(2)	1.0	1.0	1.0	
	U_{iso}	0.0032(4)	0.0032(4)	0.011(2)	0.023(4)	0.012	
	x	0	0	0	0	0.25	0.75
	y	0	0	0	0	0.25	0.25
0.3	z	0.3621(1)	0.3621(1)	0	0.1721(7)	0.0	0.0
	Frac	0.77(2)	0.23(2)	1.0	1.0	1.0	1.0
	U_{iso}	0.0052(3)	0.0052(3)	0.010(1)	0.014(3)	0.012	0.012
	x	0	0	0	0	0.25	0.75
	y	0	0	0	0	0.25	0.25
0.5	z	0.3612(1)	0.3612(1)	0	0.1709(9)	0.0	0.0
	Frac	0.62(2)	0.37(2)	1.0	1.0	1.0	1.0
	U_{iso}	0.0060(5)	0.0060(5)	0.008(1)	0.019(3)	0.012	0.012
	x	0	0	0	0	0.25	0.75
0.7	y	0	0	0	0	0.25	0.25
Phase 1	z	0.3609(3)	0.3609(3)	0	0.174(2)	0.0	0.0
49 wt. %	Frac	0.55(3)	0.45(3)	1.0	1.0	1.0	1.0
	U_{iso}	0.0051(6)	0.0051(6)	0.006(2)	0.017(6)	0.012	0.012
	x	0	0	0	0	0.25	0.75
0.7	y	0	0	0	0	0.25	0.25
Phase 2	z	0.3603(3)	0.3603(3)	0	0.168(2)	0.0	0.0
51 wt. %	Frac	0.51(3)	0.49(3)	1.0	1.0	1.0	1.0
	U_{iso}	0.0051(6)	0.0051(6)	0.006(2)	0.017(6)	0.012	0.012
	x	0	0	0	0	0.25	0.75
1.0	y	0	0	0	0	0.25	0.25
Phase 1	z	0.3613(10)	0.3613(10)	0	0.162(8)	0.0	0.0
12 wt. %	Frac	0.73(13)	0.27(13)	1.0	0.75(10)	1.0	1.0
	U_{iso}	0.006(1)	0.006(1)	0.008(2)	0.006(5)	0.012	0.012
	x	0	0	0	0	0.25	0.75
1.0	y	0	0	0	0	0.25	0.25
Phase 2	z	0.3608(2)	0.3608(2)	0	0.165(1)	0.0	0.0
88 wt. %	Frac	0.33(3)	0.67(3)	1.0	1.00(1)	1.0	1.0
	U_{iso}	0.006(1)	0.006(1)	0.008(2)	0.006(5)	0.012	0.012

TABLE IV. Selected bond distances in $La_{2-x}Sr_xNiO_{4+\delta}$. Note that (1) calculated e.s.d.'s for O_{basal} are low due to positional constraints and (2) bond distances do not reflect O_{basal} positional disorder.

	Sr(0.1)	Sr(0.3)	Sr(0.5)	Sr(0.7) Phase 1 49 wt. %	Sr(0.7) Phase 2 51 wt. %	Sr(1.0) Phase 1 12 wt. %	Sr(1.0) Phase 2 88 wt. %
Ni-La(Sr)	3.2420(7)	3.2256(7)	3.2220(8)	3.2233(24)	3.2242(23)	3.218(7)	3.2079(12)
	3.2432(7)	3.2273(7)	3.2263(8)	3.2229(24)	3.2247(23)		3.2083(12)
Ni-O_{basal}(1)	1.92578(4)	1.91455(6)	1.90554(6)	1.90501(16)	1.90765(14)	1.9047(5)	1.91275(24)
Ni-O_{basal}(2)		1.91550(6)	1.90888(6)	1.90812(16)	1.91419(14)	1.9070(5)	1.91361(24)
Ni-O_{apical}	2.215(11)	2.188(9)	2.176(9)	2.205(26)	2.109(23)	2.06(10)	2.041(13)
(LaSr)-O_{basal}(1)	2.6088(9)	2.5970(9)	2.6008(10)	2.5998(30)	2.5996(28)	2.594(9)	2.5754(15)
(LaSr)-O_{basal}(2)		2.5963(9)	2.5983(10)	2.5975(30)	2.5948(28)	2.592(9)	2.5747(15)
(La,Sr)-O_{apical}	2.373(11)	2.416(9)	2.424(9)	2.377(25)	2.426(22)	2.52(11)	2.425(13)
	2.7604(18)	2.7418(15)	2.7255(14)	2.732(4)	2.7248(32)	2.712(11)	2.7244(14)
O_{basal}(1)-O_{basal}(2)	2.72272(7)	2.70724(5)	2.69466(8)	2.69604(12)	2.70270(14)	2.69503(29)	2.70589(9)
O_{basal}(1)-O_{apical}	2.935(8)	2.907(7)	2.892(7)	2.914(20)	2.844(17)	2.80(7)	2.798(9)
O_{basal}(2)-O_{apical}		2.908(7)	2.894(7)	2.916(20)	2.848(17)	2.81(7)	2.797(9)

(0.75, 0.25, 0) yielded unreasonably low values of ~1.90 Å. When Ni-O_{basal} bond distances are calculated using one of the O_{basal} lobes [for example, (0.308, 0.195, 0)], the revised Ni-O_{basal} bond length is ~1.97 Å, which is chemically reasonable. Moreover, with increasing substitution of Sr for La, the bimodality of the electron density contours in the F_{obs} maps grew progressively more distinct. Thus we believe that the limitations of a powder diffraction data set inhibited an explicit refinement of the disordered oxygen positions, but crystal chemical considerations strongly support the results of the Fourier syntheses.

The octahedral rotations associated with the *d* and *l* microtwins serve to stabilize the K_2NiF_4 structure adopted by the (La,Sr) nickelates. The K_2NiF_4 compounds can be envisioned as RMO_3 perovskitelike sheets that alternate with *R*O halitelike sheets.[21] When these layers are dimensionally mismatched, one or both of these sheets must deform to maintain structural continuity. In $La_2NiO_{4+\delta}$ and $LaCuO_{4+\delta}$, long *M*-O-*M* bond distances (where *M* = Ni or Cu) in the perovskitelike layers exacerbate the mismatch.[22] In both compounds the mismatch is relieved by modification of the perovskitelike layer, which distorts so as to reduce the *M*-*M* distance without shortening the *M*-O_{basal} bond.

In both the cuprates and the nickelates, this *M*-*M* bond reduction occurs through deviations of the *M*-O_{basal}-*M* angle from 180°, but the polyhedral distortions that achieve this geometry are fundamentally different in the two compounds. In cuprates, the Cu-O_{basal}-Cu angle buckles normal to 001, effectively corrugating the CuO_2 basal plane.[23] This deformation lowers the tetragonal K_2NiF_4 symmetry to *Bmab* and deflects the O_{apical}-Cu-O_{basal} angle from 90°. Such a distortion is favorable only if the O_{apical}-Cu bond is relatively weak. By contrast, our results suggest that Ni-Ni bond shortening in the nickelates occurs by rotation of the NiO_6 octahedron as a rigid unit about the *c* axis. As noted by Mehta

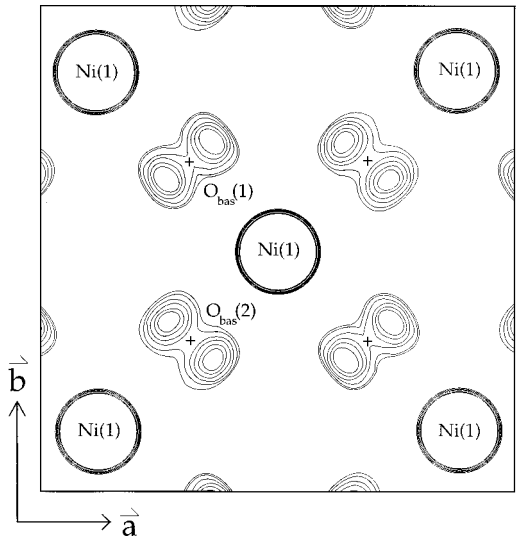

FIG. 4. An F_{obs} map of the (001) plane at $z = 0$ reveals splitting of the basal oxygen atoms in Sr(0.5). Crosses mark the centroid position used for this refinement. Peak maxima at the Ni positions have been suppressed. Electron density contours range from 0.4 to 0.9 $e^-/Å^3$.

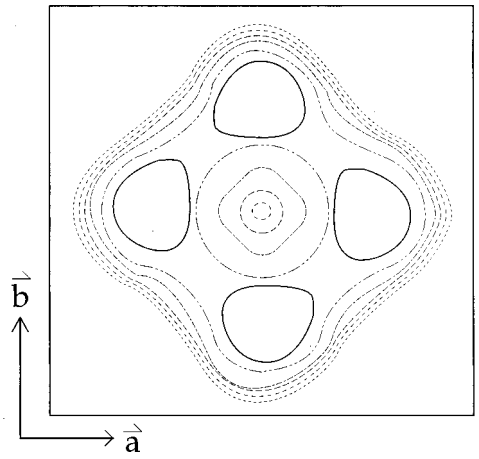

FIG. 5. An F_{obs} map parallel to the (001) plane at $z = 0.174$ in phase 1 of Sr(0.7) through the apical oxygen position. Four electron density maxima surround the central refined position at a distance of ~0.8 Å. Electron density contours range from 0.4 (smallest dashes) to 0.65 (solid line) $e^-/Å^3$.

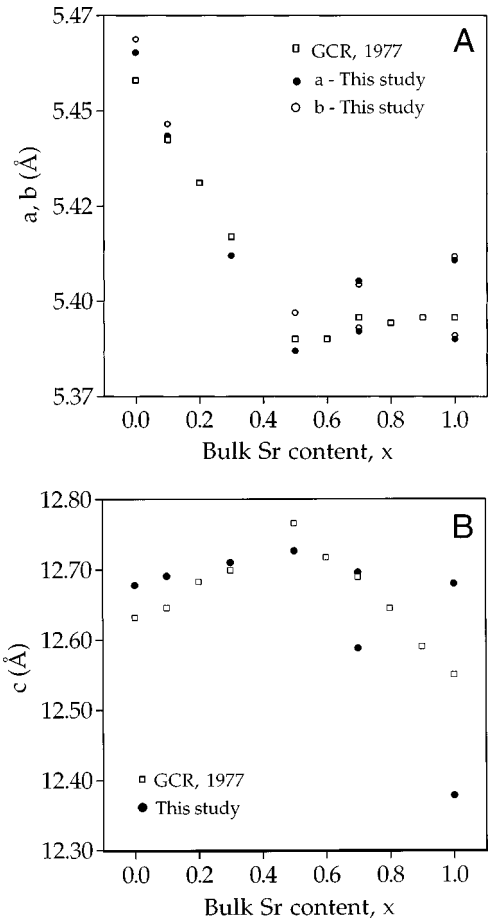

FIG. 6. Variation of lattice parameters as a function of Sr content. (A) *a* and *b* axes and (B) *c* axis. Open squares represent previously published values by Gopalakrishnan *et al.* (Ref. 5).

and Heaney,[13] this rotation lowers the symmetry to *Bbcm* and involves no deviation of the O_{apical}-*M*-O_{basal} bond angles from ideality. The preference that nickelates display for the *Bbcm* type rather than the *Bmab* type of distortion indicates that *M*-O_{apical} bonding is stronger in the nickelates than in the cuprates.

Granados *et al.*[6] have speculated that substitution of the larger Sr^{2+} cation for La^{3+} should enlarge the halitelike layer and thereby decrease the dimensional mismatch with the perovskitelike layer. This improved fit in turn should stabilize the idealized tetragonal K_2NiF_4 structure. However, the results of this and previous studies[2,5,6] reveal a complex variation in the lattice parameters with increasing *x* [Figs. 6(a) and 6(b)], such that the unit cell volume of $La_{2-x}Sr_xNiO_{4+\delta}$ *decreases* with increasing Sr content (Fig. 7). This volume reduction appears consistent with the decreasing symmetry observed in the present study for higher degrees of Sr substitution, but its cause is not clear. Structural contraction may accompany the loss of interstitial oxygen from the halitelike layer with increasing Sr concentration, or it may reflect shorter Ni-O bond distances due to the oxidation of Ni^{2+} to Ni^{3+}.

D. Phase immiscibility for $x>0.5$

The diffraction patterns for Sr(0.7) and Sr(1.0) contained split peaks that suggested the presence of two intergrown

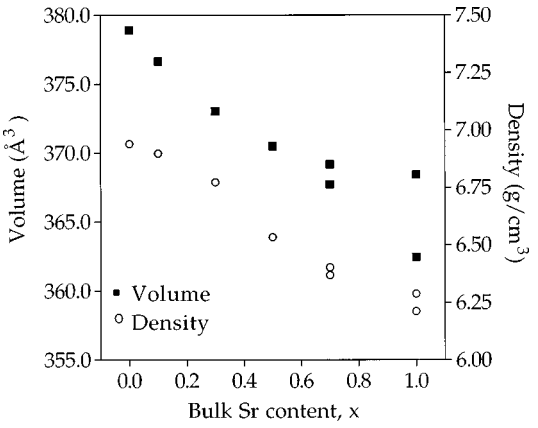

FIG. 7. Dependence of volume and density on Sr content.

phases with slightly different cell parameters (Fig. 8). In particular, the 00*l* peaks contained two distinct components that cannot be explained by a reduction in symmetry, indicating biphasic mixtures. As a result, these compositions were refined assuming two component phases. Starting values for the axis parameters were determined from direct measurements of diagnostic peaks. Severe correlation effects due to the metrically tetragonal pseudosymmetry were overcome by separation of *a* and *b* by 0.001 Å for the individual phases in Sr(0.7) and Sr(1.0) with constraints that forced equal changes to *a* and *b*. With these constraints, the refinements converged and χ^2 improved significantly from >4.0 to ~ 2.5.

The bimodal phase mixtures for Sr(0.7) and Sr(1.0) may be attributed to either of two factors: incomplete reaction during synthesis or equilibrium immiscibility at the final temperature of processing. Although the former cannot be ruled out entirely, some considerations suggest that the bimodal assemblages grew in equilibrium. An incomplete synthesis might be expected to include the starting materials ($SrCO_3$, NiO, and La_2O_3) rather than two closely related

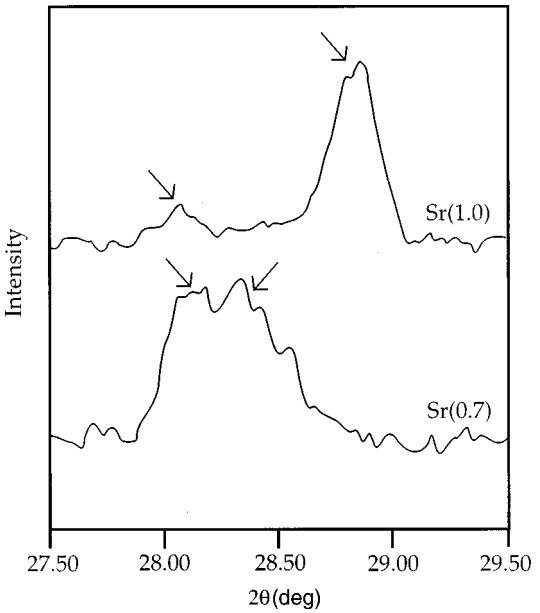

FIG. 8. Splitting of 004 peaks for Sr(0.7) and Sr(1.0) reveals the intergrowth of two phases.

phases. In addition, heating samples with high Sr contents for longer periods did not change the fraction of the secondary phase. Moreover, Jorgensen and his colleagues have described similar biphasic behavior for both $La_2CuO_{4+\delta}$ and $La_2NiO_{4+\delta}$ on the basis of neutron powder diffraction.[18,24] In the case of $La_2NiO_{4.07}$, the intergrowths comprise two closely related orthorhombic phases, with $\delta=0$ (i.e., formal Ni valence$=2.0$) and $\delta=0.12$ (i.e., formal Ni valence $=2.24$). However, the range of these Ni valence states falls outside that of the present study.

The thermochemical measurements of DiCarlo *et al.*[4] indicate that the incorporation of additional holes in $La_{2-x}Sr_xNiO_{4+\delta}$ is energetically unfavorable for $x=0.5$; by contrast, hole states are very stable for $x>0.5$. The appearance of phase immiscibility in the (La,Sr)-nickelate series coincides with this second thermochemical discontinuity, and one may interpret the observed behavior as the coexistence of two different hole states for $0.5<x<1.0$. Specifically, this biphasic regime appears to comprise a hole-saturated phase with $x<0.5$ and a Sr-rich phase with available holes. The emergence of these hole states may also explain the decrease in resistivity and the increase in the Seebeck coefficient for large values of x.[2,5,6] It is possible that this Sr-rich phase may be identified with the separate phase observed by Cava *et al.*[2] near $x=1.0$, but they discerned a bronze color to their material, while our mixtures up to $x=1.0$ remained black.

It generally is assumed that the holes induced by Sr substitution will occupy the Ni $3d$-type states (creating Ni^{3+}), in which case the Sr-rich phase observed in the biphasic regime should exhibit an increased Jahn-Teller distortion. In our analysis, however, the short Ni-O_{apical} bond length refined for the Sr-rich phase approaches the Ni-O_{basal} bond lengths in magnitude, indicating a much smaller Jahn-Teller distortion than occurs for lower Sr concentrations. This observation, coupled with the abrupt change in magnitude of the a and c lattice parameters at $x=0.5$ [Figs. 6(a) and 6(b)], may support a transfer of a Ni $3d$ valence electron from the z^2 to the x^2-y^2 orbital, as originally posited by Gopalakrishnan *et al.*[5] Alternatively, this behavior may indicate a transfer of the hole from the Ni^{3+} cation to the oxygen anion for Sr-rich compositions.

E. Polaron ordering at low temperature

Recent studies of (La,Sr) nickelate have demonstrated complex phase transition behavior below room temperature. For instance, the electron-diffraction investigation of Chen *et al.*[25] provides evidence for the appearance of an incommensurate superstructure at ~ 220 K. The behavior of the incommensurate wave vector with increasing x reveals three distinct regimes, which the authors attribute to different states of polaron ordering. Single-crystal neutron-diffraction data for $x=0.135$ and 0.20 of Sachan *et al.*[10] and Tranquada *et al.*[26] generally support the interpretations of Chen *et al.*, although these authors argue for cooperative ordering of both dopant-induced holes and Ni spins at $T\leqslant 100$ K.

The boundaries of the three wave vector regimes are comparable to those detected in this study and in the thermochemical measurements of DiCarlo *et al.*[4] Although it is tempting to equate the anomalies displayed by the incommensurate wave vector with those observed in the enthalpy of oxidation and the crystal structure, several discrepancies suggest that the phenomena are not directly related. According to the model for polaron ordering of Chen *et al.*,[25] discontinuities in the variation of the incommensurate wave vector should be correlated with discontinuities in the hole concentration (or the formal Ni valence) as a function of Sr content. As seen in Fig. 3, however, two independent measurements of hole concentration revealed no such stepwise behavior at 25 K. Further, ordering processes that occur at temperatures of ~ 200 K typically exhibit enthalpies of only 3–10 kJ/mol rather than the values of 200–300 kJ/mol observed for (La,Sr) nickelates. If charge density waves underlie the thermochemical behavior, then the ordering would have to occur at temperatures that are sufficiently high for oxidation to take place. However, the superstructures in $La_{2-x}Sr_xNiO_{4+\delta}$ described by Chen *et al.*[25] and by Sachan *et al.*[10] appear well below room temperature.

IV. CONCLUSIONS

Our results suggest that three structurally distinct regimes occur along the $La_2NiO_{4+\delta}$-$LaSrNiO_{4+\delta}$ join, and these regimes may be directly correlated to the thermochemical behavior observed by DiCarlo *et al.*[4] For $0\leqslant x<0.2$, the formal valence of Ni is relatively low, and an analysis of Ni-O bond lengths suggests that holes occupy conventional Ni^{3+}-type states. The average symmetry of this phase is $Fmmm$, although positional disorder among basal oxygen atoms indicates that $Bbcm$ is the highest symmetry possible at a local scale. The incorporation of additional holes in this phase is an exothermic process. For compounds with a moderate Ni valence ($0.2<x<0.5$), the addition of holes becomes energetically unfavorable, and the conventional Ni^{3+}-type states appear to have become saturated. This transition from an unsaturated to a saturated state is accompanied by a change from orthorhombic to monoclinic symmetry. When the formal nickel valence is greater than 2.5 (i.e., for $x>0.6$), $La_{2-x}Sr_xNiO_{4+\delta}$ decomposes into a biphasic assemblage. One of the phases of the assemblage is a hole saturated, monoclinic compound, and the other is believed to be metallic with energetically favorable hole states.

A preliminary analysis of the Ni-O bond lengths in conjunction with Seebeck and electromagnetic measurements suggests that the holes in the Sr-rich, high-Ni-valence phase are of different character from the conventional Ni^{3+}-type holes. In a study of $BaNiO_{2+y}$, DiCarlo *et al.*[27] have proposed that Ni^{3+}-type holes become ''peroxidelike'' at a formal Ni valence of 2.48. This valence is very similar to that for which holes change character in $La_{2-x}Sr_xNiO_{4+\delta}$. However, the high-valence phase of $La_{2-x}Sr_xNiO_{4+\delta}$ needs to be isolated and thoroughly investigated via thermochemical, electromagnetic, and high-resolution structural measurements before the nature of the high-valence holes in $La_{2-x}Sr_xNiO_{4+\delta}$ can be satisfactorily identified.

Finally, our results reinforce the idea that (La,Sr) nickelates are fundamentally different from their cuprate analogs. To the extent that confinement of electron holes to two-dimensional conduction planes is a requirement for superconductivity, the extreme Jahn-Teller distortions observed in the cuprates create an electronic environment that is not rep-

licated in the nickelate structures. Our refinements of the nickelates suggest that the NiO_6 octahedra in $La_{2-x}Sr_xNiO_{4+\delta}$ act as relatively rigid units: They rotate as individual polyhedra to create twin domains with *Bbcm* symmetry (for $x<0.2$). Moreover, the ratio of Ni-O_{apical} to Ni-O_{basal} reaches a maximum of only ~ 1.16 at $x=0.5$, and the small octahedral asymmetry becomes even smaller in the high-valence metallic phase. By contrast, in $La_{2-x}Sr_xCuO_{4+\delta}$ the apical oxygens essentially are isolated from the copper cations; the ratio of Cu-O_{apical} to Cu-O_{basal} is ~ 1.27 for $La_{2-x}Sr_xCuO_{4+\delta}$,[28] and the CuO_2 planes buckle to create a structure with *Bmab* symmetry. These observations strongly support a three-dimensional coordination for Ni in $La_{2-x}Sr_xNiO_{4+\delta}$, which therefore lacks the isolated two-dimensional conduction planes found in cuprates.

ACKNOWLEDGMENTS

The authors would like to thank J. DiCarlo and D. Banschick for aid in specimen synthesis. This work was supported by NSF Grant No. EAR9418031 and by DOE Grant No. DEFG02-89ER45394.

*Author to whom correspondence should be addressed.

[1] S. A. Hoffman, C. Venkatraman, S. N. Ehrlich, S. M. Durbin, and G. L. Liedl, Phys. Rev. B **43**, 7852 (1991).
[2] R. J. Cava, B. Batlogg, T. T. Palstra, J. J. Krajewski, W. F. Peck, Jr., A. P. Ramirez, and L. W. Rupp, Jr., Phys. Rev. B **43**, 1229 (1991).
[3] S. M. Hayden, G. H. Lander, J. Zaretsky, P. J. Brown, C. Stassis, P. Metcalf, and J. M. Honig, Phys. Rev. Lett. **68**, 1061 (1992).
[4] J. DiCarlo, A. Mehta, D. Banschick, and A. Navrotsky, J. Solid State Chem. **103**, 186 (1993).
[5] J. Gopalakrishnan, G. Colsmann, and B. Reuter, J. Solid State Chem. **22**, 145 (1977).
[6] X. Granados, J. Fontcuberta, M. Vallet-Regi, M. J. Sayagués, and J. M. González-Calbet, J. Solid State Chem. **102**, 455 (1993).
[7] Y. Takeda, R. Kanno, M. Sakano, O. Yamamoto, M. Takano, Y. Bando, H. Akinaga, K. Takita, and J. B. Goodenough, Mater. Res. Bull. **25**, 293 (1990).
[8] G. H. Lander, P. J. Brown, C. Stassis, P. Gopalan, J. Spalek, and G. Honig, Phys. Rev. B **43**, 448 (1991).
[9] P. J. Brown, S. M. Hayden, G. H. Lander, J. Zaretsky, C. Stassis, P. Metcalf, and J. M. Honig, Physica B **180&181**, 380 (1992).
[10] V. Sachan, D. J. Buttrey, J. M. Tranquada, J. E. Lorenzo, and G. Shirane, Phys. Rev. B **51**, 12 742 (1995).
[11] D. E. Rice and D. J. Buttrey, J. Solid State Chem. **105**, 197 (1993).
[12] A. C. Larson and R. B. von Dreele (unpublished).
[13] A. Mehta and P. J. Heaney, Phys. Rev. B **49**, 563 (1994).
[14] D. G. Peters, J. M. Hayes, and G. M. Hieftje, *Chemical Separations and Measurements* (Saunders, Philadelphia, 1974), pp. 322–332.
[15] A. I. Nazzal, V. Y. Lee, E. M. Engler, R. D. Jacowitz, Y. Tokura, and J. B. Torrance, Physica C **153**, 1367 (1988).
[16] N. F. Zakharchuk, T. P. Fedina, and N. S. Borisova, Supercond. Phys. Chem. Technol. **4**, 1282 (1991).
[17] A. K. Ganguli, R. Nagarajan, G. Ranga Rao, N. Y. Vasanthacharya, and C. N. R. Rao, Solid State Commun. **72**, 195 (1989).
[18] J. D. Jorgensen, B. Dabrowski, Shiyou Pei, D. R. Richards, and D. G. Hinks, Phys. Rev. B **40**, 2187 (1989).
[19] W. C. Hamilton, Acta Crystallogr. **18**, 502 (1965).
[20] E. Prince, in *The Rietveld Method*, edited by R. A. Young (Oxford University Press, Oxford, 1995), pp. 43–54.
[21] I. D. Brown, Z. Kristallogr. **199**, 255 (1992).
[22] C. N. R. Rao, D. J. Buttrey, N. Otsuka, P. Ganguly, H. R. Harrison, C. J. Sandberg, and J. M. Honig, J. Solid State Chem. **51**, 266 (1984).
[23] J. B. Goodenough and A. Manthiram, J. Solid State Chem. **88**, 115 (1990).
[24] J. D. Jorgensen, B. Dabrowski, Shiyou Pei, D. G. Hinks, L. Soderholm, B. Morosin, J. E. Shirber, E. L. Venturini, and D. S. Ginley, Phys. Rev. B **38**, 11 337 (1988).
[25] C. H. Chen, S.-W. Cheong, and A. S. Cooper, Phys. Rev. Lett. **71**, 2461 (1993).
[26] J. M. Tranquada, J. E. Lorenzo, D. J. Buttrey, and V. Sachan, Phys. Rev. B **52**, 3581 (1995).
[27] J. DiCarlo, I. Yazdi, A. J. Jacobson, and A. Navrotsky, J. Solid State Chem. **109**, 223 (1994).
[28] T. Kamiyam, F. Izumi, H. Asano, H. Takagi, S. Uchida, Y. Tokura, E. Takayama-Muromachi, M. Matsuda, K. Yamada, Y. Endoh, and Y. Hidah, Physica C **172**, 120 (1990).